

# Quantization of Multiparticle Auger Rates in Semiconductor Quantum Dots

V. I. Klimov,<sup>1\*</sup> A. A. Mikhailovsky,<sup>1</sup> D. W. McBranch,<sup>1</sup>  
C. A. Leatherdale,<sup>2</sup> M. G. Bawendi<sup>2</sup>

We have resolved single-exponential relaxation dynamics of the 2-, 3-, and 4-electron-hole pair states in nearly monodisperse cadmium selenide quantum dots with radii ranging from 1 to 4 nanometers. Comparison of the discrete relaxation constants measured for different multiple-pair states indicates that the carrier decay rate is cubic in carrier concentration, which is characteristic of an Auger process. We observe that in the quantum-confined regime, the Auger constant is strongly size-dependent and decreases with decreasing the quantum dot size as the radius cubed.

Excitation of a gas-phase or near-surface atom can eject a low-lying electron and leave a “hole” state within the atomic levels. A higher lying electron can recombine with this hole state, and the energy released in electron-hole (e-h) recombination can be emitted as a photon (radiative decay) or as an electron in the nonradiative Auger process (1). The Auger process also occurs in bulk semiconductors (2), in which the emitted (reexcited) particle can be either an electron or a hole.

The efficiency of Auger processes, which are mediated by Coulomb electron-electron interactions, differs greatly between the atomic and bulk semiconductor cases. In atomic systems, for which the electron-electron coupling is much stronger than the electron-photon coupling, the rates of Auger transitions are significantly greater than the rates of the radiative transitions. As a result, the decay of the multi-electron states in atomic systems is dominated by Auger processes. The efficiency of Auger effects is greatly reduced in bulk materials because of the reduced Coulomb electron-electron coupling and kinematic restrictions imposed by energy and momentum conservation. We used nearly monodisperse colloidal nanoparticles [quantum dots (QDs)] of different sizes to study confinement-induced modifications in Auger-type interactions during the transformation from bulk crystalline to atomic regimes.

Three-dimensional carrier confinement results in discrete atomiclike energy spectra of QDs (3–5) and modification of multiparticle interactions, including those due to Auger effects (6–9). Confinement-induced en-

hancement in Coulomb interactions and relaxation in the translation momentum conservation should lead to increased Auger rates (6, 7) in comparison with those in bulk materials, whereas the atomiclike structure of energy levels in QDs should hinder Auger processes because of the reduced availability of final states satisfying energy conservation. As a result, Auger recombination can only occur efficiently with the participation of a phonon (as a four-particle process) or with the involvement of a final state from the continuum of states outside the QD (Auger ionization) (6, 10). The complex interplay between the above effects complicates a theoretical analysis of quantum-confined Auger recombination and highlights the need for experimental mapping of the size-dependent Auger rates.

Experimental data for the Auger effect in QDs have typically been analyzed within a bulk semiconductor approach by introducing an effective carrier concentration in the dot ( $n_{\text{eh}} = N/V_0$ , where  $N$  is the number of e-h pairs per dot and  $V_0$  is the dot volume) and a cubic carrier decay rate ( $C_A n_{\text{eh}}^3$ , where  $C_A$  is the Auger constant) (11, 12). However, it is not obvious that this approach should be valid in the regime of a few e-h pairs per dot, for which recombination occurs as a sequence of quantized steps from the  $N$  to  $N-1$ ,  $N-2$ , . . . and finally to the 1–e-h pair state (Fig. 1A). In the “quantized” regime, Auger recombination is characterized not by a continuum of density-dependent recombination times  $\tau_A = (C_A n_{\text{eh}}^2)^{-1}$  as in bulk materials, but by a set of discrete recombination constants, characteristic of the decay of the 2-, 3-, . . . e-h pair QD states.

We quantitatively studied quantum-confined Auger recombination in cadmium selenide (CdSe) colloidal QDs with mean radii  $R$  ranging from 1 to 4 nm and with size dispersion ranging from 4 to 7%. The average QD populations were monitored with 100-fs

time resolution using a high-sensitivity transient absorption (TA) experiment. This experiment allowed us to detect carrier-induced absorption changes ( $\Delta\alpha$ ) over the 400- to 950-nm spectral range with an accuracy up to  $10^{-5}$  in differential transmission (13). At excitation densities of one to four pairs per dot, we observed clear quantization of the relaxation rates measured for different multiple-pair states. The TA data indicate that in the quantum-confined regime, the Auger relaxation times vary strongly with QD radius as  $R^3$ .

As a measure of instant QD populations, we used the carrier-induced absorption bleaching ( $\Delta\alpha < 0$ ) of the lowest 1S optical transition. Because of extremely fast (subpicosecond) energy relaxation in QDs (14), the bleaching decay on time scales longer than 1 ps is not affected by intraband dynamics and is entirely due to population changes of the QD quantized states (15). In Fig. 1B, we show spectra of  $\Delta\alpha d$  ( $d$  is the sample thickness) of QDs with  $R = 2.8$  nm detected at 2 ps after excitation at initial carrier densities  $\langle N_0 \rangle$  from 0.8 to 8 e-h pairs per dot on average (these spectra as well as other data shown below were taken at room temperature). QD average populations were calculated by using the expression  $\langle N_0 \rangle = j_p \sigma_0$ , where  $j_p$  is the pump photon fluence, and  $\sigma_0$  is the QD absorption cross section determined as described in (16). The dotted line in Fig. 1B shows the linear absorption spectrum  $\alpha_0$ . Because of the narrow size distribution of the QDs, both the linear absorption and nonlinear absorption (bleaching) spectra show atomiclike discrete features corresponding to interband optical transitions involving different electron and hole quantized states [for explanation of the states’ labeling see (17)]. Increasing pump levels led to progressive bleaching of the optical transitions, primarily due to state-filling associated with increasing population of the 1S and 1P electron states (18).

In Fig. 1C (symbols), we show the normalized 1S absorption bleaching ( $-\Delta\alpha/\alpha_0$ ) plotted versus  $\langle N_0 \rangle$  for QDs of different radii. The 1S absorption change grew linearly at low pump intensities ( $\langle N_0 \rangle < 0.5$ ) and saturated as  $-\Delta\alpha/\alpha_0$  approached unity at high pump densities. In the representation  $-\Delta\alpha/\alpha_0$  versus  $\langle N_0 \rangle$ , the samples of all sizes from 1 to 4 nm showed identical pump-dependent behavior, which can be fit to the “universal” curve  $-\Delta\alpha/\alpha_0 = k_1 \langle N_0 \rangle / (k_2 + \langle N_0 \rangle)$  with  $k_1 = 1.05 \pm 0.15$  and  $k_2 = 1.6 \pm 0.3$  (line in Fig. 1C). In our studies, we used this expression to translate the measured  $\Delta\alpha(t)$  dynamics into dynamics of QD average populations  $\langle N(t) \rangle$ .

In Fig. 1D (main panel and lower inset), we show the normalized QD population dynamics for a 2.8-nm sample measured at carrier injec-

<sup>1</sup>Chemical Science and Technology Division, CST-6, MS-J585, Los Alamos National Laboratory, Los Alamos, NM 87545, USA. <sup>2</sup>Department of Chemistry and Center for Materials Science and Engineering, Massachusetts Institute of Technology, 77 Massachusetts Avenue, Cambridge, MA 02139, USA.

\*To whom correspondence should be addressed. E-mail: klimov@lanl.gov

## REPORTS

tion levels  $\langle N_0 \rangle$  from 0.5 to 3.5. Over this range of excitation densities, the temporal evolution of  $\langle N \rangle$  is dominated by contributions from QDs in 4-, 3-, 2- and 1-e-h pair states:  $\langle N(t) \rangle \approx [4n_4(t) + 3n_3(t) + 2n_2(t) + n_1(t)]/n_{\text{QD}}$ , where  $n_{\text{QD}}$  is the total density of QDs in the sample, and  $n_N$  ( $N = 1$  to 4) is the concentration of QDs

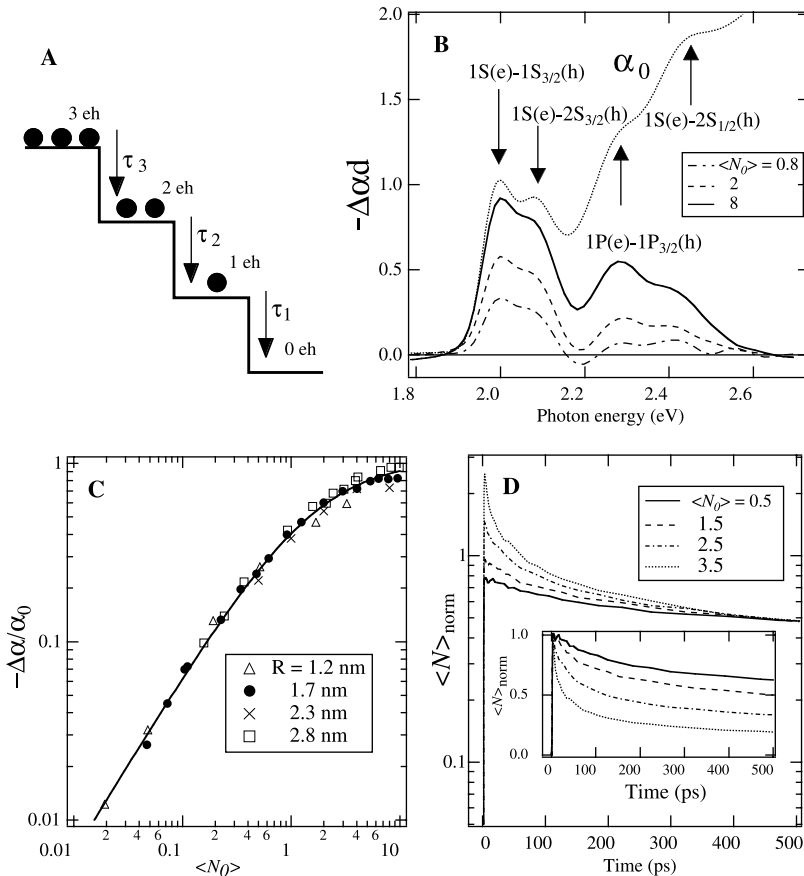
having  $N$  e-h pairs. The QD multiparticle dynamics can be described by the set of coupled rate equations (19) with a straightforward solution given by a sum of exponential terms as follows:  $\langle N(t) \rangle = \sum_{N=1}^4 A_N e^{-t/\tau_N}$ , where  $A_N$  is time-independent coefficients determined by initial injection densities and  $\tau_N$  is the lifetime

of the  $N$ -pair QD state. At low pump intensities ( $\langle N_0 \rangle < 1$ ), the population relaxation is dominated by the decay of singly excited QDs (term  $A_1 e^{-t/\tau_1}$ ). Increasing pump density results in the consecutive "turn-on" of exponential terms, accounting for the decay of QDs in 2-, 3-, ... e-h pair states.

We developed a simple subtractive procedure to extract single exponential dynamics that are characteristic of the decay of different multiple-pair QD states from the measured  $\langle N(t) \rangle$  time transients (20). Using this procedure, we could extract the dynamics of up to the 4-pair state while still keeping the noise level below 20 to 25% of the signal amplitude. The validity of the subtractive procedure was verified by a direct comparison with the results of numerical integration of the rate equations (19). The multiple-pair lifetimes determined by these two complementary approaches deviated only by 10 to 20%.

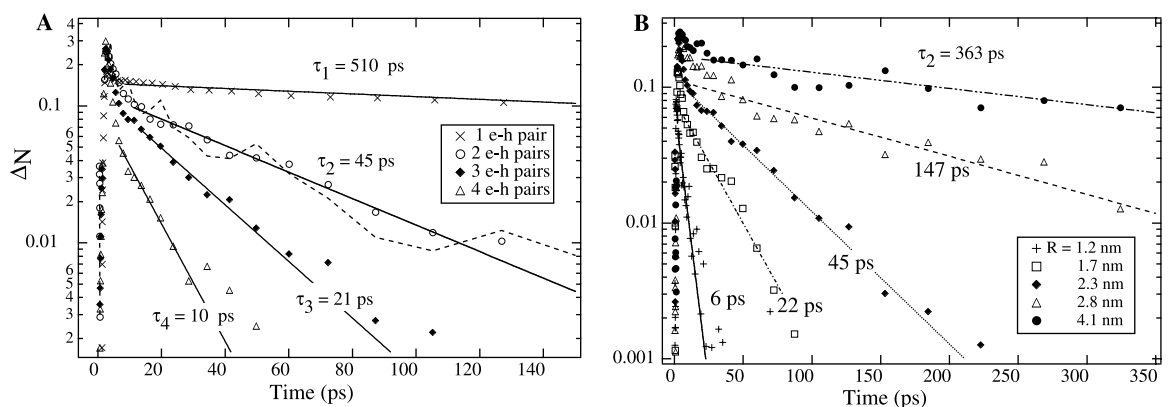
The extracted dynamics of the 2-, 3-, and 4-pair states (Fig. 2A;  $R = 2.3$  nm) indicate that the carrier decay becomes progressively faster as the number of e-h pairs per dot increases, as expected for Auger recombination. In bulk semiconductor arguments, the effective decay time constant  $\tau_N$  in the Auger regime is given by  $\tau_N^{-1} = C_A(N/V_0)^2$  ( $N \geq 2$ ). This expression predicts a ratio  $\tau_4:\tau_3:\tau_2 = 0.25:0.44:1$  which is very close to the ratio 0.22:0.47:1 of experimentally determined times of 4-, 3-, and 2-pair relaxation (10, 21, and 45 ps, respectively). The quantitative match of scaling for the multiparticle relaxation times indicates that the decay rates for quantum-confined Auger recombination are cubic with respect to the carrier density ( $dn_{\text{eh}}/dt \propto -n_{\text{eh}}^3$ ), just as in bulk materials.

In Fig. 2B, we compare the two-pair decay dynamics for QDs of different sizes. The  $\tau_2$  time constant decreased from 363 to 6 ps when the dot radius was reduced from 4.1 to 1.2 nm, indicating a cubic size dependence  $\tau_2 \propto R^3$  (Fig. 3A, circles). The time constants



**Fig. 1.** (A) Quantized steps in quantum-confined Auger recombination in QDs. (B) Pump-dependent TA spectra of CdSe QDs ( $R = 2.8$  nm) detected at 2 ps after excitation in comparison to linear absorption spectrum; arrows indicate the positions of optical transitions coupling various electron and hole quantized states [see (17)]. (C) "Universal" pump dependence of the normalized 1S bleaching for QD samples with  $R = 1.2, 1.7, 2.3,$  and  $2.8$  nm (symbols); the line is a fit to  $k_1 \langle N_0 \rangle / (k_2 + \langle N_0 \rangle)^{-1}$ , with  $k_1 = 1.05$  and  $k_2 = 1.6$ . (D) Pump-dependent dynamics of QD average populations  $\langle N(t) \rangle$  normalized to match either their long-term decay values (main panel) or their initial amplitudes (lower inset).

**Fig. 2.** (A) Dynamics of 1-, 2-, 3-, and 4-e-h pair states (symbols) extracted from TA data for the 2.3-nm sample [see text and (20)], fit to a single exponential decay (solid lines); circles and the dashed line are 2-pair decay dynamics extracted from TA data taken at  $\langle N_0 \rangle = 1.6$  and 1.3, respectively. (B) 2-e-h pair dynamics for QD samples with radii 1.2, 1.7, 2.3, 2.8, and 4.1 nm (symbols), fit to a single exponential decay (lines).



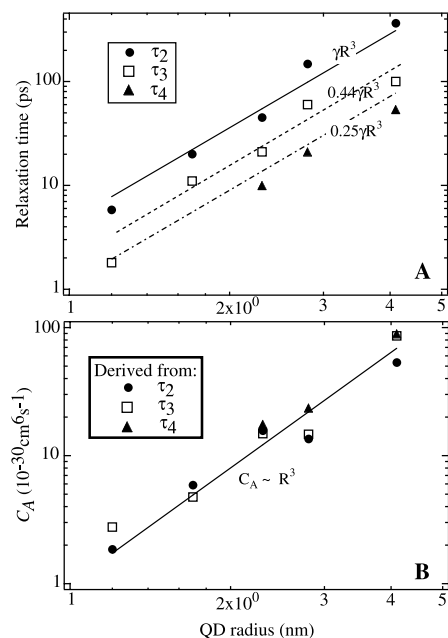


**Fig. 3.** (A) Size dependence of relaxation constants of 2-, 3-, and 4-e-h pair states (symbols), fit to the dependencies  $\gamma R^3$ ,  $0.44\gamma R^3$ , and  $0.25\gamma R^3$ , respectively (lines);  $\gamma$  is a size-independent constant. (B) Size dependence of the Auger constant (symbols), fit to the dependence  $C_A \propto R^3$  (line); circles, squares, and triangles correspond to data derived from the lifetimes of the 2-, 3-, and 4-pair states, respectively.

measured for the 3- and 4-pair decay (Fig. 3, squares and triangles) followed the same size dependence as that of the 2-pair state, so that the time-constant ratios predicted by the bulk semiconductor model held for all QD sizes [compare lines (model) and symbols (experimental data) in Fig. 3A]. Simple bulk material reasoning would suggest that the enhancement in the Auger decay in smaller particles is caused by an effective increase in carrier concentrations resulting from the increased spatial confinement. However, the  $R^3$  size dependence of relaxation times measured experimentally is different from the  $R^6$  dependence predicted by the bulk semiconductor model, which shows that in QDs, the Auger “constant” depends on the particle size, as also indicated by calculations of QD Auger ionization (6). The Auger constant derived from the relaxation data decreases with reducing QD radius as  $R^3$  from  $\sim 7 \times 10^{-29} \text{ cm}^6 \text{ s}^{-1}$  for  $R = 4.1 \text{ nm}$  to  $\sim 2 \times 10^{-30} \text{ cm}^6 \text{ s}^{-1}$  for  $R = 1.2 \text{ nm}$  (Fig. 3B). For all QD sizes, the  $C_A$  values calculated by using lifetimes of 2-, 3-, and 4-e-h pair states are close to each other (compare data shown by circles, squares, and triangles in Fig. 3B), indicating that the cubic density dependence of the Auger rates holds for all sizes between 1 and 4 nm.

We used QD samples with different surface passivations to study the effect of QD surface/interface properties on Auger rates. In

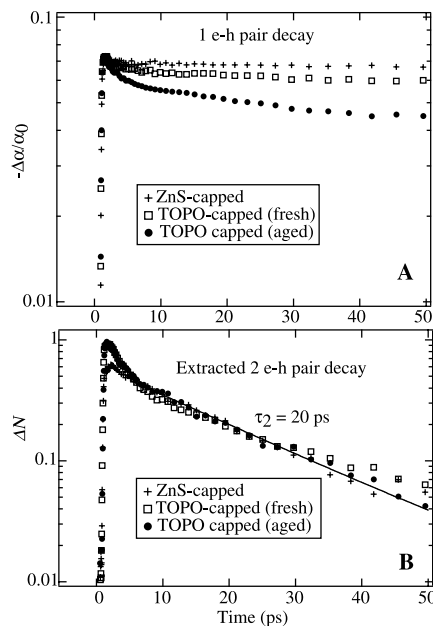


**Fig. 4.** (A) The low pump intensity 1S bleaching dynamics ( $\langle N_0 \rangle = 0.11$ ) for CdSe QDs ( $R = 1.7 \text{ nm}$ ) with differently prepared surfaces: fresh (squares) and aged (circles) TOPO-capped QD samples and a sample of QDs overcoated with a ZnS layer (crosses). (B) 2-e-h pair decay for the same set of samples.

Fig. 4, we show 1-pair (Fig. 4A) and 2-pair (Fig. 4B) dynamics for 1.7-nm CdSe QDs either capped with molecules of tri-*n*-octylphosphine oxide (TOPO) [squares (freshly prepared sample) and circles (aged sample)] or overcoated with four monolayers of ZnS (crosses). As indicated by photoluminescence quantum-yield measurements of these three samples, the best surface passivation was provided by the epitaxial ZnS layer. Freshly prepared TOPO-capped samples had a lower degree of surface passivation, which was further reduced upon sample aging. TA data taken at  $\langle N_0 \rangle = 0.11$  (Fig. 4A) show that the reduction in the degree of surface passivation leads to faster initial dynamics of the single e-h pair state, indicating that these dynamics are affected by trapping at surface defects. In contrast, the 2-e-h pair decay (Fig. 4B) is not significantly altered by changing surface or interface properties, which strongly suggests that Auger recombination in the samples studied is dominated by processes involving QD volume (quantized) states, without a substantial contribution from Auger ionization.

**References and Notes**

1. D. Chatterji, *The Theory of Auger Transitions* (Academic Press, London, 1976).
2. P. Landsberg, *Recombination in Semiconductors* (Cambridge Univ. Press, Cambridge, 1991).
3. A. Alivisatos, *Science* **271**, 933 (1996).
4. D. J. Norris, A. Sacra, C. B. Murray, M. Bawendi, *Phys. Rev. Lett.* **72**, 2612 (1994).
5. D. Gammon, E. Snow, B. V. Shanabrook, D. Katzer, D. Park, *Science* **273**, 87 (1996).
6. D. Chepic *et al.*, *J. Lumin.* **47**, 113 (1990).

7. A. L. Efros, V. A. Kharchenko, M. Rosen, *Solid State Commun.* **93**, 281 (1995).
8. J. L. Pan, *Phys. Rev. B* **46**, 3977 (1992).
9. C. Delerue, M. Lannoo, G. Allan, E. Martin, *Phys. Rev. Lett.* **75**, 2228 (1995).
10. A. Efros and M. Rosen, *Phys. Rev. Lett.* **78**, 1110 (1997).
11. M. Ghanassi, M. Schanne-Klein, F. Hache, A. Ekimov, D. Ricard, *Appl. Phys. Lett.* **62**, 78 (1993).
12. V. Klimov and D. McBranch, *Phys. Rev. B* **55**, 13173 (1997).
13. ———, *Opt. Lett.* **23**, 277 (1998).
14. ———, *Phys. Rev. Lett.* **80**, 4028 (1998).
15. In (14), subpicosecond intraband energy relaxation was observed in the low pump intensity regime (less than 1 e-h pair per dot on average). For the multiparticle regime studied in this work, relaxation should be even faster because of the increasing efficiency of Auger-type energy transfer processes (7) (these intraband processes are different from the interband Auger recombination studied here).
16. V. I. Klimov, D. W. McBranch, C. A. Leatherdale, M. G. Bawendi, *Phys. Rev. B* **60**, 13740 (1999).
17. In spherical QDs, electron states are labeled as  $nL$ , where  $L = S, P, D$ , etc. is the atomiclike notation for the angular momentum of the electron envelope wave function, and  $n$  is the number of the state of a given symmetry. A similar notation is used for hole states, with the addition of a subscript that denotes the total hole angular momentum, which is the sum of the valence-band Bloch-function momentum and the momentum of the hole envelope wave function [for example, see (4)].
18. S. Hunsche, T. Dekorsy, V. Klimov, H. Kurz, *Appl. Phys. B* **62**, 3 (1996).
19. The decay of multiple-pair states in QDs via a sequence of quantized steps (Fig. 1A) can be described by the following set of coupled rate equations:
 
$$\frac{dn_N}{dt} = -\frac{n_N}{\tau_N} \frac{dn_{N-1}}{dt} = \frac{n_N}{\tau_N} - \frac{n_{N-1}}{\tau_{N-1}} \dots$$

$$\frac{dn_1}{dt} = \frac{n_2}{\tau_2} - \frac{n_1}{\tau_1}.$$
 If we neglect recombination during the pump pulse (a reasonable approximation with our 100-fs pump pulses), the initial conditions for the above equations can be calculated using the Poisson distribution
 
$$n_m(t=0) = n_{\text{QD}} \frac{\langle N_0 \rangle^m}{m!} e^{-\langle N_0 \rangle},$$

$$m = 1, 2, \dots N$$
20. We extract single-exponential multiparticle dynamics by normalizing the time transients so that the long-time decay values match (at long times after photoexcitation, the decay is governed by singly excited QDs, independent of the initial carrier density) (Fig. 1D). We subtract the low pump intensity trace ( $\langle N_0 \rangle < 1$ ; single e-h pair decay) from traces recorded at  $\langle N_0 \rangle > 1$ , which yields dynamics  $\Delta N(t)$  due to relaxation of multiple-pair states with  $N \geq 2$ . For initial carrier densities  $1 < \langle N_0 \rangle < 2$ , this procedure yields the two-pair state dynamics (circles in Fig. 2A), with a faster initial component due to contribution from states with a larger number of excited pairs. The two-pair decay is further subtracted (after normalization) from the  $\Delta N(t)$  time transients detected at  $\langle N_0 \rangle > 2$  to derive dynamics of states with  $N \geq 3$ . This procedure can be repeated to extract dynamics of QD states with  $N = 4, 5$ , etc. The results for the extracted  $N$ -pair decay were not sensitive to the exact magnitude of the initial QD populations taken between  $N - 1$  and  $N$ , as illustrated in Fig. 2A by comparison of 2-pair dynamics derived from traces recorded at  $\langle N_0 \rangle = 1.6$  (circles) and 1.3 (dashed line).
21. Supported by Los Alamos Directed Research and Development funds under the auspices of the U.S. Department of Energy. C.A.L. and M.G.B. also acknowledge partial funding from the NSF-MRSEC program under grant DMR-9400334.

21 September 1999; accepted 3 December 1999